Article

Deposition of Different Metallic Coatings as Repair Materials for Concrete by Using a Twin-Wire Arc Thermal Spray Process

Sang Youl Kim [1], Han-Seung Lee [2,*] and Jin-Ho Park [3,*]

1   Department of Architectural Engineering, Hanyang University, Seongdong-gu, Seoul 04763, Republic of Korea
2   Department of Architectural Engineering, Hanyang University ERICA, Sangnok-gu,
    Ansan 15588, Republic of Korea
3   Department of Research Promotion Team, Hanyang University ERICA, Sangnok-gu,
    Ansan 15588, Republic of Korea
*   Correspondence: ercleehs@hanyang.ac.kr (H.-S.L.); jhpark9422@hanyang.ac.kr (J.-H.P.);
    Tel.: +82-31-400-5181 (H.-S.L.); +82-31-400-4847 (J.-H.P.)

Abstract: Using a concrete surface, the ingress of aggressive ions and the initiation of the corrosion reaction of an embedded steel rebar were studied. To reduce the corrosion reaction of the embedded steel rebar, either a coating on the steel rebar or a repair material was used on the concrete surface. Therefore, in the present study, 200 μm thick Cu, Ti, and 85Zn-15Al were used as repair materials, and their coatings were deposited on the concrete surface using a twin-wire arc thermal spray process. Different experiments such as bond adhesion, water permeability, immersion in a 5 wt.% NaCl solution, and accelerated carbonation were performed to assess the durability of the coatings, and the characterization of the coatings was performed by using scanning electron microscopy (SEM) and X-ray diffraction (XRD). The Cu and 85Zn-15Al coatings exhibited severe defects and porosity; therefore, these coatings exhibited very low bond adhesion, whereas the Ti coating showed a dense and compact morphology, and its bond adhesion value was 11 times greater than that of the Cu coating. The NaCl immersion results can be used to determine the extent of the deterioration of different coatings in coastal areas; based on these results, the Cu coating exhibited delamination, while 85Zn-15Al showed white rust deposition. By contrast, there was no detrimental effect of NaCl immersion on the Ti coating during the 28 days under study, and the coating exhibited characteristics identical to those observed after deposition. The Ti coating reduced the carbonation depth by 1.5–2 times that of the Cu and 85Zn-15Al coatings after four and eight weeks of exposure. The present study suggests that Ti can be the potential metal used as a repair material for concrete to enhance the durability of buildings and infrastructure.

Keywords: coating; concrete; arc thermal spray; repair materials; scanning electron microscopy; X-ray diffraction

1. Introduction

The spalling and collapse of buildings and infrastructure are mainly caused by the corrosion of embedded steel rebars in the concrete. In this case, the corrosion products formed inside the concrete cause internal pressure; therefore, the delamination of reinforced concrete (RC) structures occurs. This is due to the poor quality of the materials used, an improper mixture design, an irregular construction process, poor workmanship, and the cover depth of the steel rebar during installation. Therefore, it is necessary to use proper repair materials to avoid the aforementioned problems in RC structures to enhance their safety and extend their service life.

There is a huge investment in the repair of RC structures worldwide. In the USA, the repair of old buildings was estimated to cost 90 billion dollars in 2016 [1], and in Europe, the costs were approximately half of the construction budget [2]. Due to rapid urbanization and industrialization, RC structures suffer from immature distress; therefore, there is a

continuous demand for repair materials for the restoration of buildings and infrastructure. Repair materials still cannot guarantee long-term effectiveness [3], as most repair materials fail within 20 years of their service. This is attributed to their weak interfacial bonding with the concrete substrate [4], but they can extend the service life and durability of buildings and infrastructure.

Another concern involves the properties of the repair material and the concrete interface needed to achieve high-quality structural repair [5]. Moreover, the interface between the repair material and the concrete substrate is a weak zone. Therefore, researchers have attempted to address these issues by considering the compatibility of different repair materials with concrete, given that most repair materials shrink owing to the difference in their chemical composition and thermal coefficients [6–8]. Repair materials should exhibit good mechanical performance, strong bond adhesion [9], and chemical resistance to improve the performance of concrete structures. It is suggested in the European standard (EN1504-3) that the bond adhesion of a repair material must be at least 0.8 MPa [10]. Cement-based materials, such as Portland cement, sulfoaluminate cement, and magnesium phosphate cement (MPC) blended with fly ash, blast furnace slag, and silica fume, are the most widely used materials. Such repair materials require a hydration reaction (curing condition) but due to the unavailability of water (non-curing) on concrete surfaces, they suffer from weak bonding and easy delamination, and they exhibit high shrinkage and low flexibility [9].

Epoxy-modified cement has been used as a concrete repair material [11–13] because of its better bonding adhesion [14]. However, it exhibits poor mechanical properties attributed to the unhardened epoxy resin remaining in the mixture, which hinders the hydration reaction [15]. Liu et al. used asphalt-modified sulfoaluminate cement as a repair material in concrete and mortar samples [16], where they exhibited a negative effect on bonding. In this case, since the concrete surface had large-size pores, it caused weak bonding, resulting in the delamination of the repair material [17].

The use of polymers as concrete repair materials causes the fading and peeling of the coating owing to the difference in the thermal coefficients of concrete and polymers. Stainless steel has been used as a repair material to protect wastewater reservoirs from deterioration [18]. In one study, a stainless steel coating was applied on a concrete surface via an arc thermal spray process, which exhibited excellent corrosion resistance in a sulfuric acid solution, attributed to the formation of Cr^{3+}-enriched Cr_2O_3 as a passive film [19]. In another study, Ti was used as an anti-corrosion and anti-ozone metal and acted as a repair material for concrete [20]. Ti coatings have excellent corrosion and ozone resistance compared with other metallic coatings deposited through the thermal spray process [19,20]. However, the bond adhesion between a metallic coating and a concrete substrate is excellent. Zn-Al coatings are used in construction to protect steel structures from corrosion; a maximum of 10% Al in a hot-dip galvanized Zn coating is acceptable to obtain good resistance [21]. The arc thermally sprayed Zn-Al coating showed superior performance in terms of corrosion resistance in an aggressive solution, which was attributed to the formation of corrosion products that blocked the active centers of the coating [22,23]. An alloyed Zn-Al coating deposited through arc thermal spraying was used for the electromagnetic shielding of a concrete surface, as it absorbs electromagnetic radiation [24]. Therefore, in the present study, different metallic coatings, that is, Cu, Ti, and 85Zn-15Al films, with 200 µm thicknesses, were deposited by using a twin-wire arc thermal spray process, and their properties were characterized through scanning electron microscopy (SEM) and X-ray diffraction (XRD), and their bond adhesion, water permeability, carbonation resistance, and 5 wt.% NaCl solution resistance were assessed.

2. Materials and Methods

2.1. Deposition of the Coatings on the Concrete Surface

Different 200 µm thick metallic coatings, namely Cu, Ti, and 85Zn-15Al, were used as repair materials and deposited on a concrete surface through a twin-wire arc thermal spray process. A rectangular concrete sample was prepared using ordinary Portland cement with

3.15 g/m^3 density and a 25 mm coarse and 5 mm fine aggregate size. The water-to-binder (W/B) ratio was maintained at 0.5. The concrete samples were cured in water for 28 days, after which the coatings were deposited. There was no pre-treatment on the concrete surface before coating deposition. The coatings were deposited using twin metal wires with a 1.6 mm diameter [19,25]. For this process, 99.95% Cu and commercially pure Ti were used to deposit the Cu and Ti coatings, while an 85%Zn-15%Al alloy wire was used to deposit the 85Zn-15Al coating. The coatings were deposited by melting the wires (metals and alloys) at 30 V and 200 mA while keeping the concrete substrate 25 cm away from the spray gun [26–29].

2.2. Bond Adhesion Measurement

The bond strength of the deposited coating on the concrete surface was measured by selecting a 40 mm × 40 mm area at different locations, following the KS F4716 Standard [30]. Before measuring the coating bond adhesion, epoxy was applied on the surface and dried for 24 h [31]. Subsequently, the extent of adhesion was determined using a Proceq DY-216 instrument. A schematic of the bond adhesion measurements is shown in Figure 1.
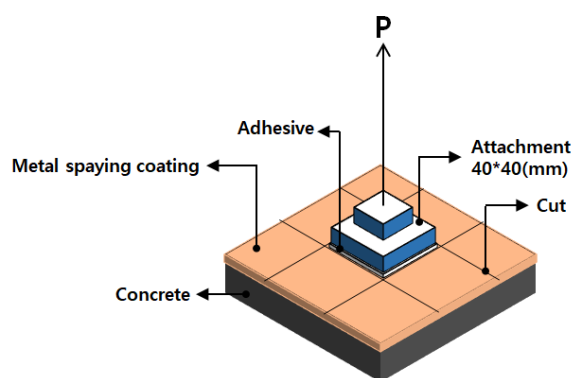

Figure 1. Schematic for bond adhesion measurement.

2.3. Characterization of Coatings and Corrosion Products

The surface morphologies of the deposited coatings and the corrosion products formed after immersion in a 5 wt.% NaCl solution for the 28 days of the test was examined with a field-emission scanning electron microscope (FE-SEM; HITACHI S-4800, Tokyo, Japan) operated at 15 kV. The coating and corrosion products were prepared using a platinum sputter (HITACHI MC1000, Tokyo, Japan) for 5 min to avoid the charging effect. The concrete surface led to vacuum loss in the instrument; therefore, it is necessary to dry the coatings and corrosion products to ensure better image quality.

The phases formed after the coating deposition and the corrosion products formed in a 3.5 wt.% NaCl solution was determined through X-ray diffraction (XRD; Rigaku, Tokyo, Japan) using Cu Kα radiation (λ = 1.5406 Å) at 40 kV and 200 mA.

2.4. Performance Evaluation of the Coatings as Repair Materials

2.4.1. Water Permeability

A water permeability test was performed by ponding/immersing the coating samples into a water tank. In this process, five sides of the samples were sealed with epoxy, and the top/coating surface (upper portion) of the samples was kept open for water penetration [20]. A 0.3 N/mm^2 pressure was applied through compressed air on the samples for 3 h. Finally, the coating samples were retrieved from the water tank, and moisture was removed using filter paper. The water permeability was measured by the weight difference in the coating samples before and after water immersion. The permeability ratio was calculated according to the KS F4930 [32] standard as follows:

$$\text{Permeability ratio} = \frac{\text{Amount of water permeated into the coating (g)}}{\text{Amount of water permeatied into the concrete (g) withut coating}} \quad (1)$$

2.4.2. Carbonation Resistance

The carbonation resistance properties of the coatings were determined by keeping the samples in 5 ($\pm$0.2)% CO_2 at 60 ($\pm$5)% relative humidity and 20 ($\pm$2) °C temperature for eight weeks according to KS F2584 [33]. The samples were stored in a carbonation chamber (Chom Dan Scientific Ind. Co., Seoul, Korea) and periodically opened for observation after spraying the phenolphthalein solution for discoloration. Five sides (except the coated surface) of the concrete were sealed with an epoxide to avoid the diffusion of CO_2 from these sides. The corrosion of coatings under carbonation conditions is generally a slow process; therefore, the samples were kept for eight weeks to assess their performance.

2.4.3. NaCl Resistance

The corrosion resistance of the coatings was assessed by immersing them in a 5 wt.% NaCl solution for four weeks while sealing the five sides of the concrete surface, and then the characterization of the corrosion products was performed to determine their nature and morphological characteristics associated with corrosion resistance in sea conditions. The digital images of the top surface (coated layer) were captured using a mobile device to observe the color change and deposition of corrosion products on the coating surface.

3. Results and Discussion

3.1. Characterization of Coatings

Briefly, 200 ($\pm$10) μm thick Cu, Ti, and 85Zn-15Al coatings were deposited on the concrete surface through an arc thermal spray process to assess their properties and durability as repair materials used in construction to reduce or delay the onset of corrosion initiation. The thicknesses of the different metallic coatings on the concrete surface were determined using an Elcometer456 (Tokyo, Japan) at four different locations.

3.1.1. SEM of the Coatings

The surface morphologies of the deposited coatings, as characterized by SEM, are shown in Figure 2. The Cu coating showed the presence of micro- and macropores along with splats [34,35], which led to the formation of severe defects (Figure 2a). There were many semi-molten metal particles of different shapes, such as globular, disk, and plate, which caused irregularities in the morphology of the coatings. By contrast, a comparison of the Ti coating morphology with that of Cu showed a uniform and compact structure [19] with inflight particles, as shown in Figure 2b. The melting point of Ti is very high; therefore, the completely molten metal particles become suspended in the atmosphere, settle during the cooling process, and partially oxidize the coating. Some splat particles are observed in Figure 2b, owing to the sudden cooling of the molten metal particles, which were later deposited on the surface and caused defects. The 85Zn-15Al alloy coating exhibited severe defects and pore formation, as shown in Figure 2c. This is attributed to the different metals used in the coating, that is, Zn and Al, which have different melting points and densities. Al has a high melting point and low density, compared with Zn; therefore, it melts at high temperatures and is deposited later owing to its low density [34], leading to the creation of defects. Moreover, if the molten Zn particles cool down with Al, it is possible to obtain a less defective coating; however, owing to atmospheric conditions, they are difficult to cool down simultaneously. Therefore, this coating exhibited severe defects along with splats and inflight particles of different sizes. The surface morphology of the coatings was correlated with cross-sectional SEM images, as shown in Figure 3. The thickness of the coating was found to be 200 ($\pm$10) μm, which correlated well with the thickness measured by using an Elcometer. Some defects were observed in the Cu coating (Figure 3a), while the Ti coating exhibited a dense morphology (Figure 3b). Therefore, this coating could exhibit

a greater bonding strength (the details are discussed in Section 3.1.3). However, 85Zn-15Al revealed severe defect formation (Figure 3c) along with a color contrast owing to the Zn and Al metals. Due to the uneven morphology of the Cu, Ti, and 85Zn-15Al coatings, the porosity of the coatings was determined using the ImageJ software by considering the cross-sectional SEM images (Figure 3). The 85Zn-15Al coating exhibited a surface porosity of 14.59%, followed by Cu (11.56%) and Ti (1.69%) coatings. The Ti coating reduced the porosity by 8.63 and 6.84 times the porosity of the 85Zn-15Al and Cu coatings, respectively. This is due to the high melting point of Ti, causing all metal particles to be completely melted, and the metal droplets become very small; therefore, they fill the open pores and enhance the properties of the coating.
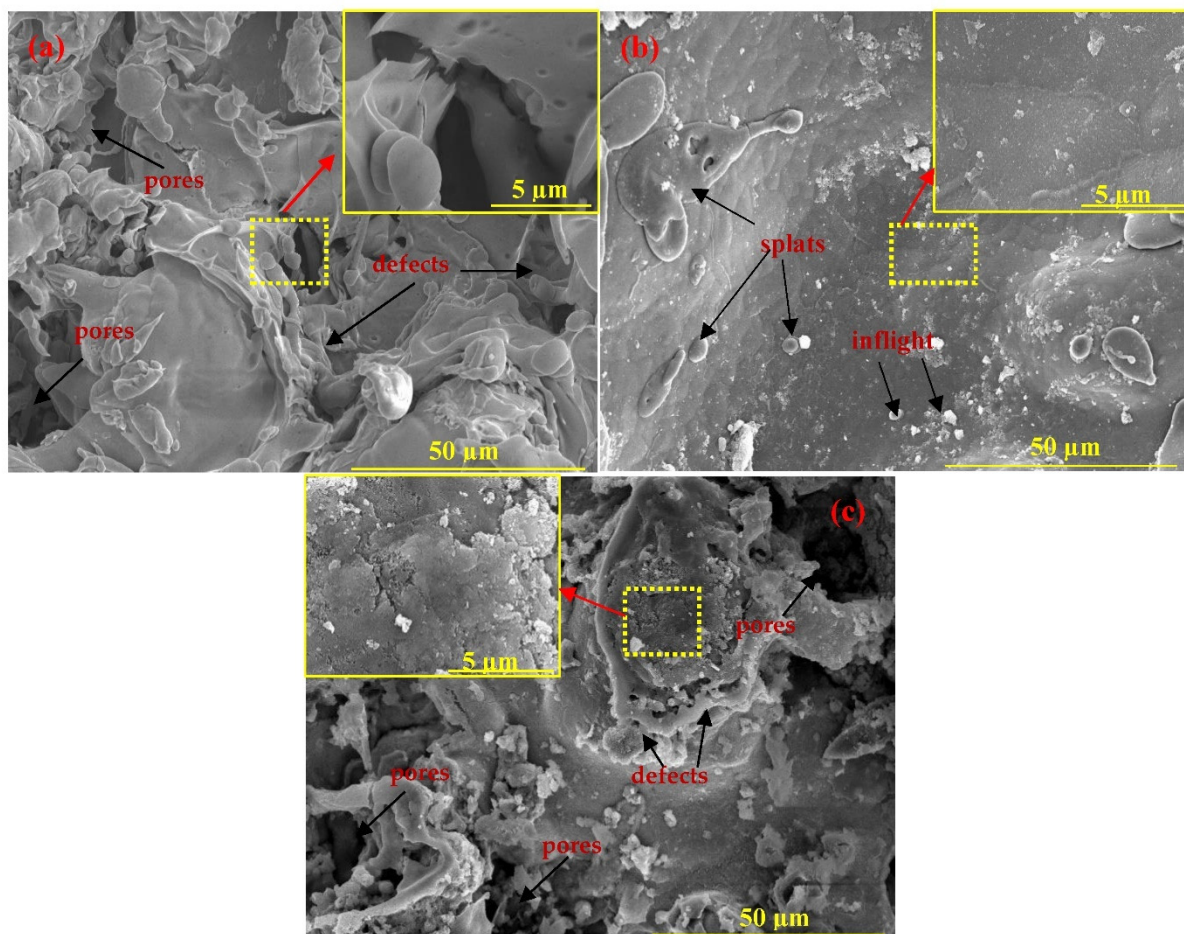

Figure 2. SEM of (**a**) Cu, (**b**) Ti, and (**c**) 85Zn-15Al coatings at 1000× and 10,000× (inset SEM images) deposited on the concrete surface.

The EDS analysis results of the coatings are listed in Table 1. As the melting point of the metal increased, the O (oxygen) content increased. The Ti coating exhibited 19.85% O, whereas 85Zn-15Al showed 2.63% O. It is possible that during the melting of the metals during the twin-wire arc thermal spray process, they were partially oxidized. The Zn and Al contents after the deposition of the 85Zn-15Al alloy coating were 84.15% Zn and 13.24% Al. The Zn content was identical to that present in the 85Zn-15Al alloy wire (feedstock). This result suggests that the O content in this coating was due to the partial oxidation of Al rather than Zn. This means that the metal with a higher melting point was oxidized during this process.
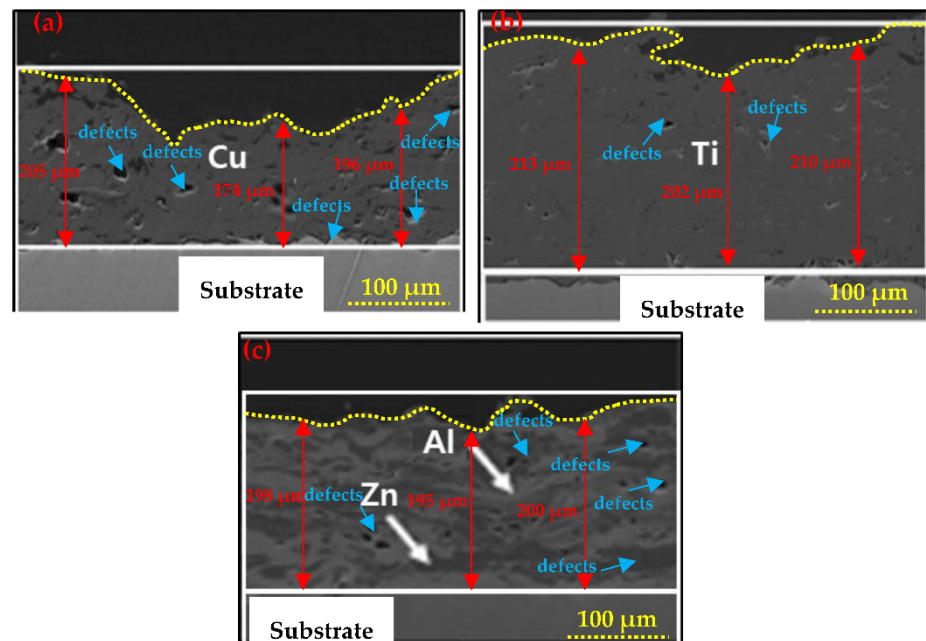
Figure 3. Cross-section SEM of (**a**) Cu, (**b**) Ti, and (**c**) 85Zn-15Al coatings at 500×.

Table 1. EDS analysis of the coatings.

Sample ID	Elements (wt.%)				
	Cu	**Ti**	**Zn**	**Al**	**O**
Cu	94.84	-	-	-	5.16
Ti	-	80.15	-	-	19.85
85Zn-15Al	-	-	84.13	13.24	2.63

3.1.2. XRD of the Coatings

EDS analysis revealed that the Cu and Ti coatings were partially oxidized; therefore, oxidation likely occurred. The phases formed during this process, along with the respective JCPDS number after the deposition of the coating, were determined via XRD, and the results are shown in Figure 4. No oxides were formed in the 85Zn-15Al coating, neither in the Zn (JCPDS:87-0713) nor in the Al (JCPDS:85-1327) phase. By comparison, a slight oxidation of the Cu coating occurred owing to the atomization of molten metal particles in the air [36], which was confirmed through EDS; therefore, it showed very small intensity peaks of Cu_2O (JCPDS:77-0199) with the Cu (85-1326) phase. Our finding is corroborated by those of Sharifahmadian et al., who observed Cu_2O along with the Cu phase [35] in a Cu coating deposited via an arc thermal spray process. The oxygen content in EDS was found to be 5.16%, which meant that the coating was partially, rather than completely, oxidized. The Ti coating was completely oxidized, owing to its high melting point; therefore, there was no Ti in the coating. This coating showed TiO (JCPDS:72-0020) and Ti_3O (JCPDS:76-1644) phases. The oxygen content in EDS was very high, which corroborates the XRD results, according to which the Ti coating exhibited oxidation.

The volume fraction (V_f%) of each phase present in the coatings was determined using the JADE software built with XRD data. The results are listed in Table 2. Notably, 19.04% Cu_2O was observed in the Cu coating, while no oxides of Zn or Al were found in the 85Zn-15Al coating. There is a possibility that native oxidation occurred, but due to the limitation of the XRD analysis, it was not observed. Most importantly, the content, that is, V_f% of the Zn and Al phases, was almost identical to that observed in the EDS analysis. No Ti was observed owing to its oxidation during the coating process. Ti_3O and TiO were

26.05% and 73.95%, respectively. Ti is oxidized either because of its high melting point or its free energy to form oxides with atmospheric oxygen [37,38].
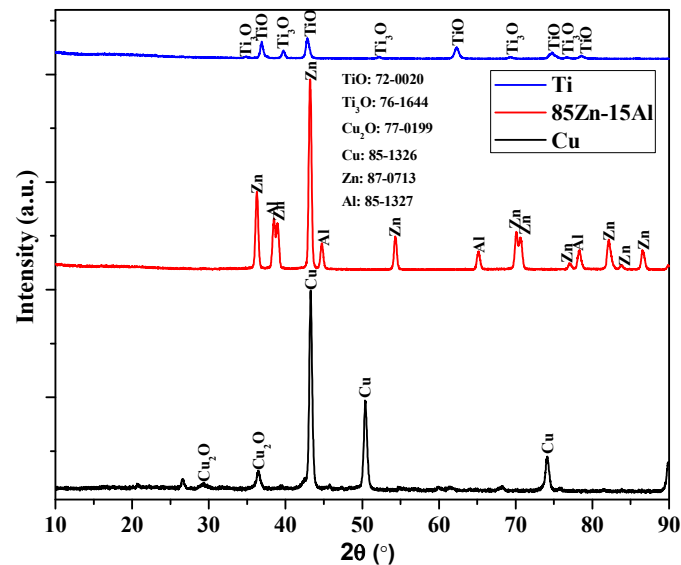

Figure 4. XRD of the coatings.

Table 2. V_f (%) of the phases.

Coatings	V_f (%)					
	Cu	Cu$_2$O	Zn	Al	TiO	Ti$_3$O
Cu	80.96	19.04	-	-	-	-
Ti	-	-	-	-	73.95	26.05
85Zn-15Al	-	-	86.25	13.75	-	-

3.1.3. Bond Adhesion Measurement

The bond adhesion values of the metallic coatings deposited on the concrete surface are shown in Figure 5. The bond adhesion values of Cu were found to be very low, i.e., 0.25 ($\pm$0.02) MPa, even lower than the minimum value recommended in KS F4716 [30], which is 1.1 MPa, and EN1504-3 [10], which is 0.8 MPa. The concrete surface exhibited very low toughness; therefore, the energy dissipation from the molten metal particles was negligible for transferring the heat from the metal to the concrete [39,40]. The interfacial bonding of the Cu coating with the concrete surface was very weak; therefore, it exhibited minimum bond adhesion values. Moreover, this result agrees well with the surface and cross-sectional morphology of the coating, which revealed severe defects and pore formation. Defects and pores lead to the destabilization of the interfacial bonding between metal and concrete. However, the 85Zn-15Al coating satisfied the minimum bond adhesion values recommended by KS F4716 and EN1504-3. This coating also exhibited defects and pores; however, owing to the low melting point and high density of Zn, it adhered to the concrete surface first. In this case, Zn completely melted after which the Al started to melt at the arcing point, thus filling the voids and defects of the 85Zn-15Al coating and enhancing its bonding strength [22]. In contrast, the Ti coating exhibited the highest bond adhesion value, which was much higher than those mentioned in earlier standards. The bond adhesion value of Ti was found to be 2.72 ($\pm$0.24) MPa. It was almost 11 and 2 times higher than those of the Cu and 85Zn-15Al coatings, respectively. This is attributed to the dense and uniform coating morphology, as observed in Figure 3b, which leads to a smaller interfacial space between Ti and the concrete surface [41]. Therefore, Ti properly adhered to the concrete surface and improved the bond adhesion.
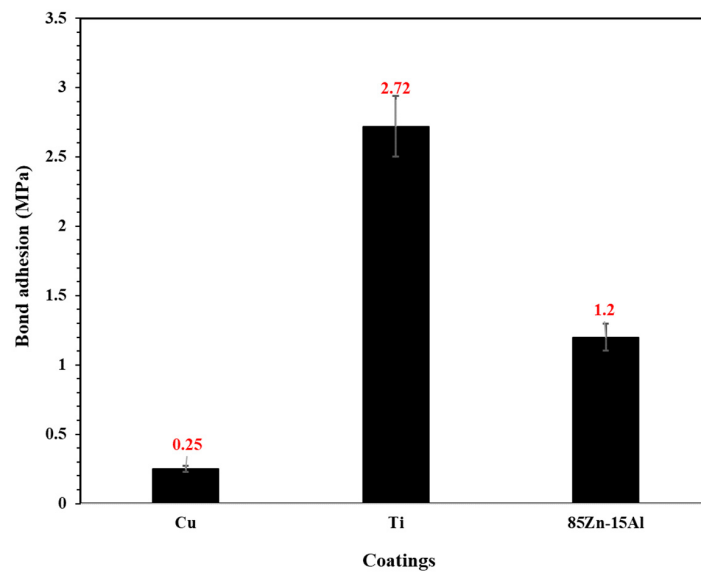
Figure 5. Bond adhesion measurement.

3.2. Performance Evaluation of the Coatings

3.2.1. NaCl Immersion Test

The deposited coatings were immersed in a 5 wt.% NaCl solution to determine their corrosion performance before and after immersion. The digital images of the coating surfaces before and after 28 days of immersion are shown in Figure 6. The Cu coating exhibited delamination (Figure 6a) due to the instability of Cu_2O and Cu in seawater [42], even though the concrete surface was still visible after immersion. After immersion in the NaCl solution, the color of the coating surface became light brown. This coating dissolved in the NaCl solution, and the color of the solution became blue-green (the figure is not shown) after 28 days of immersion owing to the dissolution of Cu and Cu_2O and the formation of copper chloride, that is, $CuCl_2$. By comparison, slight fading was observed in the Ti coating, as shown in Figure 6b. This result suggests that the NaCl solution did not have a significant effect on the deterioration of the Ti coating because of the formation of Ti_3O and TiO as oxide films, which resisted the ingress of the solution owing to their stability. The 85Zn-15Al coating exhibited the deposition of white rust on the surface, as shown in Figure 6c. The deposition of a white rust layer could be attributed to the formation of $ZnO/Zn(OH)_2/Zn_5(OH)_8Cl_2 \cdot H_2O$. The nature of the oxide film was confirmed with the XRD analysis used for the characterization of the corrosion products, as indicated in Section 3.3.2.

Figure 6. Digital images of (**a**) Cu, (**b**) Ti, and (**c**) 85Zn-15Al in 5% NaCl solution after 28 days of immersion.

3.2.2. Carbonation Resistance

The carbonation depth (mm) and digital images of the coatings after four and eight weeks of exposure are listed in Table 3. The concrete surface (without coating) exhibited 14.4 and 18 mm penetration of CO_2, and discoloration was mostly observed on the outer surface. With the increase in the exposure periods, the penetration depth increased because of the porous nature of the concrete surface, owing to the easy ingress of CO_2. Moreover, an interesting observation in the Cu coating was that the CO_2 penetration depth was higher than that without coating (concrete) even after four and eight weeks, which was attributed to the lower bond adhesion, the greater affinity of Cu with CO_2 (chemical reactivity), and porous surface morphology, which causes CO_2 to easily penetrate and reach beneath the coating. This result suggests that the Cu coating cannot function as a barrier to the ingress of CO_2 even though it accelerates the carbonation reaction. The Cu coating had a penetration depth of 20.2 mm after eight weeks of exposure. In comparison, the Ti coating exhibited the lowest penetration depth, at 9.2 mm after four weeks and 12.5 mm after eight weeks. This is attributed to its dense and compact morphology, as shown in Figures 2b and 3b, and oxide formation, which restricts the movement/diffusion and chemical reaction of CO_2. The carbonation depth results were in good agreement with those of the surface morphology, where the Ti coating exhibited the least porosity and a dense microstructure (Figure 3b), resulting in the least penetration of CO_2. The 85Zn-15Al coating after four weeks of exposure showed a 13.3 mm penetration, which was lower than that without coating (only concrete); however, once the exposure period was extended to eight weeks, it exhibited the highest penetration, that is, 21.2 mm. This might be attributed to the porous nature of the corrosion products, as CO_2 easily penetrates and reacts with Zn or Al, thus forming oxides, which later initiate the corrosion of the steel rebar embedded in the concrete. Owing to the high reaction affinity of Zn with CO_2 to form hydrozincite ($Zn_5(CO_3)_2(OH)_6$), it showed the highest CO_2 penetration depth after eight weeks of testing. The present findings suggest that Cu and 85Zn-15Al cannot be used as repair materials due to their high CO_2 penetration. By contrast, the Ti coating exhibited an almost 1.5–2 times lower CO_2 penetration even after four and eight weeks of exposure. This means that Ti can be used as a repair material for concrete and can extend the service life of exposed structures in industrial areas.

Table 3. CO_2 penetration depth and resistance measurement.

Sample ID	4 Weeks	8 Weeks
Concrete	14.4 mm	18 mm
Cu	14.8 mm	20.2 mm

Table 3. *Cont.*

Sample ID	4 Weeks	8 Weeks
Ti	9.2 mm	12.5 mm
85Zn-15Al	13.3 mm	21.2 mm
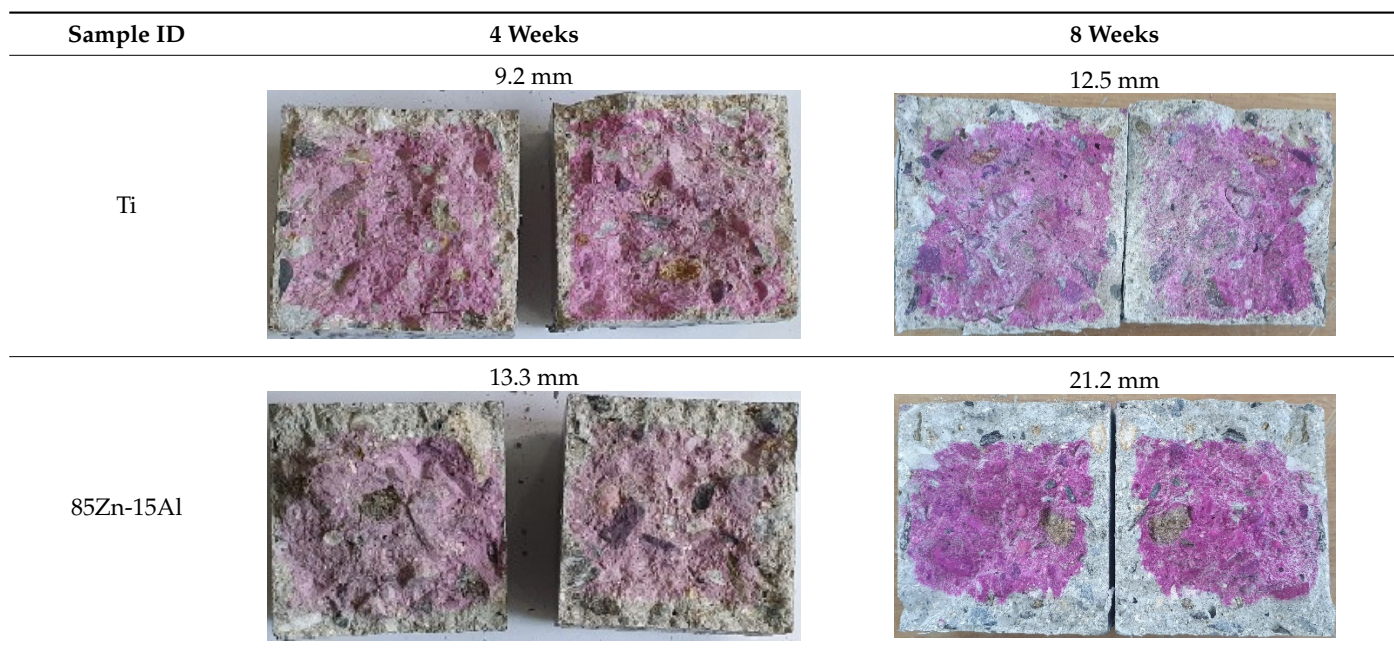
3.2.3. Water Permeability

The amount of water that penetrated the concrete and the permeability ratio are listed in Table 4. The amount of water that penetrated the concrete (without coating) showed the highest value of 22.9 g, owing to the direct penetration of water through the open pores of the concrete in which no barrier (i.e., coating) was applied. By contrast, once the coatings were deposited on the concrete surface, all the coatings exhibited almost twice the reduced amount of water penetration during the test. The Ti coating showed the lowest water absorption and permeability owing to its dense and uniform morphology, whereas Cu exhibited the highest. This finding is well-corroborated by the bond adhesion, accelerated carbonation, and NaCl immersion results, where Ti exhibited excellent performance, followed by 85Zn-15Al and Cu. Therefore, it was necessary to characterize the surface morphology and nature of the corrosion products formed after immersion in a 5% NaCl solution (the most aggressive environment) by using SEM and XRD, respectively.

Table 4. Water permeability measurement.

Coatings	Weight of Samples before Water Immersion (g)	Weight of Samples after Immersion in Water (g)	Amount of Water Permeated (g) = Weight of Samples after Water Immersion—Weight of Samples before Water Immersion	Permeability Ratio
Concrete	802.3	825.2	22.9	-
Cu	785.2	798.0	12.8	0.56
Ti	885.1	896.7	11.6	0.50
85Zn-15Al	815.4	827.8	12.4	0.54

3.3. Characterization of Corrosion Products after 28 Days of Immersion in a 5% NaCl Solution

3.3.1. SEM of Corrosion Products

The surface morphology of the corrosion products after 28 d of immersion in a 5% NaCl solution is shown in Figure 7. The globular Cu particles observed in Figure 7a suggest the formation of copper oxides or chlorides because the solution became blue-green. This assumption was confirmed with the EDS and XRD analyses of the corrosion products. The

details are described in subsequent sections. In addition to the globular shape, the concrete surface revealed coating delamination. This result was in good agreement with the digital images shown in Figure 6a, which illustrates the concrete surface and some Cu particles. In comparison, the Ti corrosion products were homogenous and uniformly covered the surface with fine particles (Figure 7b), which filled the remaining pores, as observed after the deposition of the coating (Figure 3b). The corrosion products formed on the 85Zn-15Al coating exhibited filamentous, globular, and flake-like morphologies (Figure 7c). The globular and flake-shaped morphologies might be attributed to the formation of simonkolleite ($Zn_5(OH)_8Cl_2$), while a needle structure reveals active Zn particles in the coating [31,43,44]. As the corrosion products were also defective, the ingress of aggressive ions, that is, Cl^- and CO_3^{2-} ions from the atmosphere, is also possible. Therefore, the 85Zn-15Al coating exhibited the highest penetration depth of CO_2 after eight weeks of exposure (Table 3).
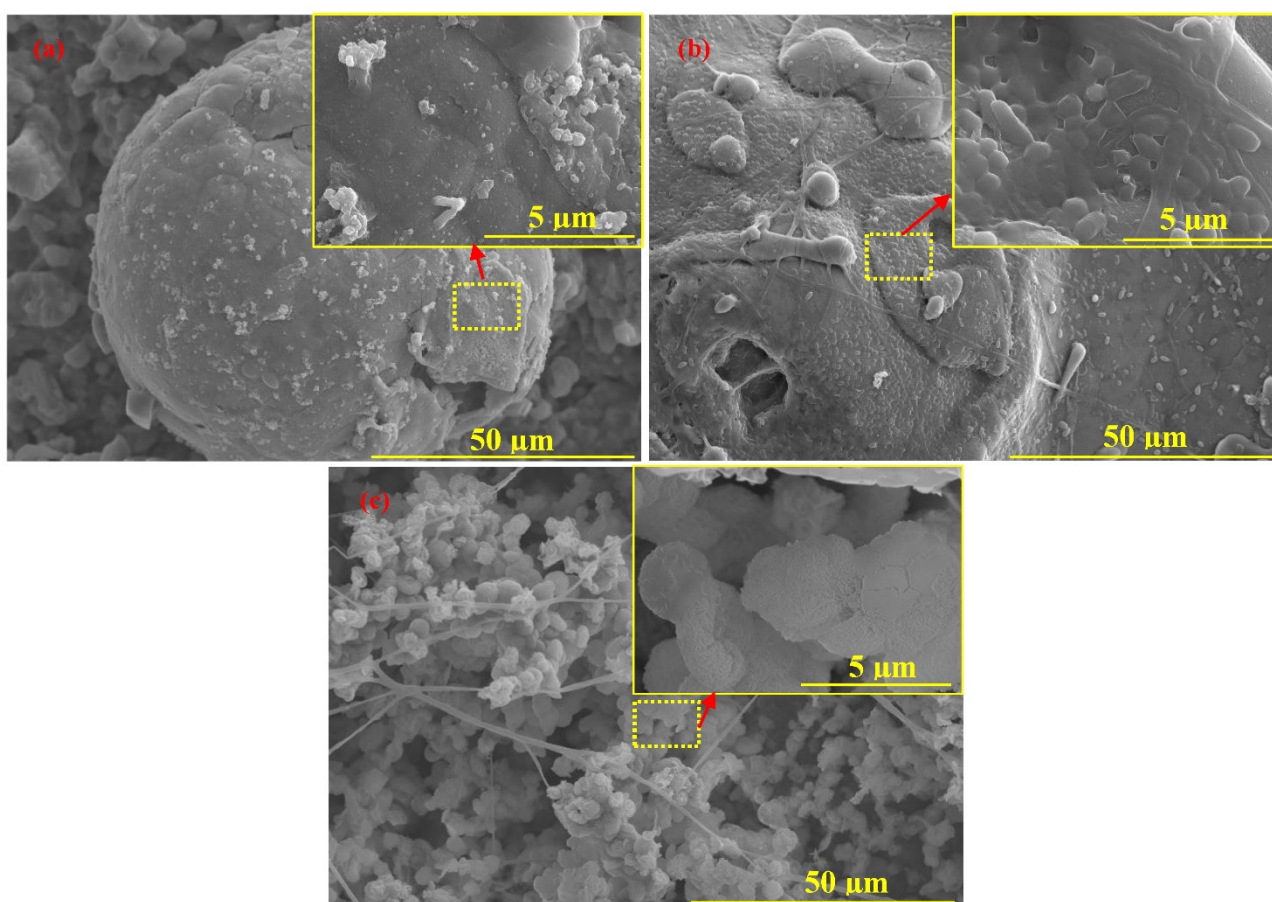

Figure 7. SEM of corrosion products formed on (**a**) Cu, (**b**) Ti, and (**c**) 85Zn-15Al coatings after 28 days of immersion in 5 wt.% NaCl solution.

The EDS analysis results of the corrosion products are listed in Table 5. The amount of Cu in the corrosion products decreased by more than twice (Table 5) that in the coating (Table 1). This result suggests that Cu was delaminated from the concrete surface; therefore, a slight amount, that is, 1.24% Ca, was observed (Table 5). This result was corroborated by the images obtained after immersion in the NaCl solution (Figure 6). The high amounts of Na and Cl revealed the deposition of NaCl, which led to the formation of copper chloride as a corrosion product (this was confirmed by XRD, as indicated in the subsequent paragraph). However, the amount of O remained identical to that observed after the coating application. This means no oxidation occurred in the coating after immersion in the NaCl solution for 28 days, in contrast to delamination and dissolution. Ti corrosion products exhibited

a slight reduction in their total content compared with that of the coating. Na and Cl were in nominal amounts, suggesting the averting nature of Ti or its oxide to interact with NaCl. In the case of the 85Zn-15Al corrosion products, the amount of Zn was reduced by almost twice the amount of the coating, revealing the deterioration of Zn compared with Al, which is attributed to the galvanically active nature of Zn. Na and Cl were also found in significant amounts, suggesting the formation of complex compounds. The reduction in the amount of Al due to the deposition of a thick corrosion product, as shown in Figure 6, hindered detection.

Table 5. EDS analysis of corrosion products formed in 5 wt.% NaCl solution after 28 days of immersion.

Coatings	Elements (wt.%)							
	Cu	Ti	Zn	Al	O	Na	Cl	Ca
Cu	46.17	0	0	0	5.26	24.38	22.96	1.24
Ti	0	77.01	0	0	22.40	0.39	0.21	0
85Zn-15Al	0	0	41.48	10.97	26.70	12.99	7.86	0

3.3.2. XRD of the Corrosion Products

The XRD results of the corrosion products after 28 d of immersion in a 5% NaCl solution are shown in Figure 8. The Cu phase disappeared in the corrosion products of the Cu coating, which was attributed to the delamination of the coating or the formation of thick corrosion products, which hindered the formation of the coating. However, Cu_2O remained in the coating after immersion in the NaCl solution. This means that Cu_2O was not dissolved in the solution. Along with Cu_2O, CuO and $CuCl_2(H_2O)_2$ were also formed as corrosion products. The formation of $CuCl_2(H_2O)_2$ corroborated the EDS analysis, based on which Cl was present in high amounts. NaCl was found in the corrosion products of the Cu coating, suggesting that it penetrated the defects/pores of the coating and filled them, as detected by XRD. No phases other than TiO and Ti_3O were observed in the corrosion products of the Ti coating. These phases were identical to those found in the Ti coating after deposition. This result indicates that NaCl does not affect the deterioration of Ti coatings deposited via a twin-wire arc thermal spray process. In contrast, the corrosion products of the 85Zn-15Al coating were Zn and Al along with simonkolleite ($Zn_5(OH)_8Cl_2 \cdot H_2O$) and NaCl. Simonkolleite is typically formed in the corrosion products of Zn when exposed to saline conditions [43]. NaCl filled the defects and pores of the corrosion products, as corroborated by the SEM images (Figure 7c) and observed by XRD.

The V_f (%) values of each phase of the corrosion products, as detected by XRD, are listed in Table 6. The V_f value of Cu_2O was almost identical to that observed after the coating application, suggesting its stability. As observed in the XRD plots, there was no Cu, which means it was delaminated or transformed into other phases. Therefore, CuO, $CuCl_2(H_2O)_2$, and NaCl were observed. $CuCl_2(H_2O)_2$ and NaCl were 48.92% and 11.50%, respectively. This result is well-corroborated with the EDS analysis results, according to which Na and Cl were in the highest amounts. TiO and Ti_3O were the corrosion products of the Ti coating and were found to be 78.54% and 21.46%, respectively. There was a slight increase in the V_f of TiO and a reduction in Ti_3O, indicating the greater stability of TiO. Therefore, at longer exposure durations, the Ti coating would be highly resistant to corrosion, thus acting as a protective layer in buildings and infrastructure. The V_f of Zn in the corrosion products of 85Zn-15Al was almost reduced twice that of the coating, suggesting the severe deterioration of the coating. Moreover, the formation of 31.09% simonkolleite can provide some resistance to corrosion; however, owing to the porosity of the corrosion products, it cannot serve as a protective agent for longer durations.
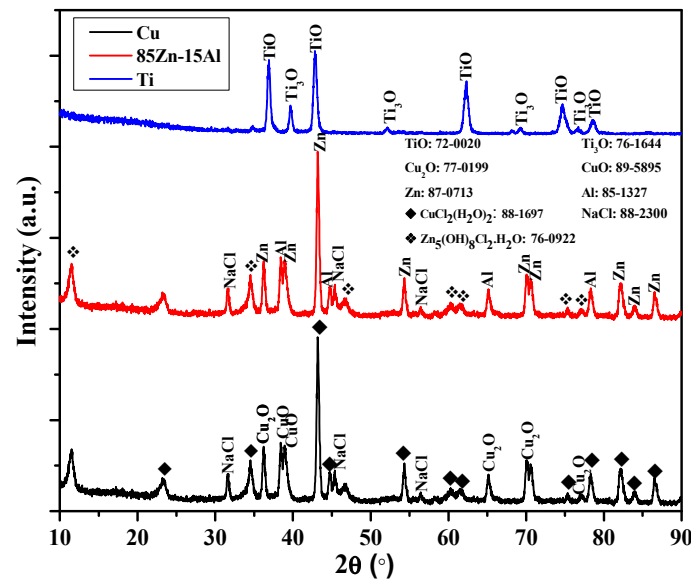
Figure 8. XRD of the corrosion products formed on the coating surface after immersion in 5% NaCl solution for 28 days.

Table 6. V_f (%) of the corrosion products.

Coatings	V_f (%)								
	CuO	Cu_2O	Zn	Al	TiO	Ti_3O	NaCl	$CuCl_2(H_2O)_2$	$Zn_5(OH)_8Cl_2 \cdot H_2O$
Cu	18.60	20.98	-	-	-	-	11.50	48.92	-
Ti	-	-	-	-	78.54	21.46	-	-	-
85Zn-15Al	-	-	45.31	12.95	-	-	10.65	-	31.09

4. Conclusions

The following conclusions were drawn in the present study:

1. The Cu and 85Zn-15Al coatings deposited through a twin-wire arc thermal spray process exhibited severe defect formation and porosity, while Ti showed a dense morphology with 1.69% porosity;

2. Cu and Ti coatings were partially oxidized owing to their high melting points, as confirmed by XRD results;

3. The Cu coating showed the lowest bond adhesion, attributed to the defects and porosity, which led to a reduction in the anchoring properties of the substrate. By contrast, the Ti coating exhibited 11 times higher bond adhesion than the Cu coating;

4. The Cu coating was susceptible to the NaCl solution, as delamination was observed on the concrete surface after 28 days of immersion, whereas the 85Zn-15Al coating formed a layer of white rust. However, NaCl did not affect the properties of the Ti coating;

5. The Ti coating exhibited around 1.5–2 times lesser carbonation penetration depth after four and eight weeks of exposure than those of the Cu and 85Zn-15Al coatings;

6. Ti could be an alternative to cement-based repair materials, polymer-modified materials, etc., as Ti-based repair materials deposited through twin-wire arc thermal spray processes extend the service life of buildings and infrastructure.

References

1. Napoli, A.; de Felice, G.; De Santis, S.; Realfonzo, R. Bond behaviour of Steel Reinforced Polymer strengthening systems. *Compos. Struct.* **2016**, *152*, 499–515. [CrossRef]
2. Climent, M.; Ortega, J.; Sánchez, I. Cement mortars with fly ash and slag—Study of their microstructure and resistance to salt ingress in different environmental conditions. In *Concrete Repair, Rehabilitation and Retrofitting III, Proceedings of the 3rd International Conference on Concrete Repair, Rehabilitation and Retrofitting (ICCRRR 2012), Cape Town, South Africa, 3–5 September 2012*; CRC Press: London, UK, 2012; pp. 3–5.
3. Alexander, M.G.; Beushausen, H.-D.; Dehn, F.; Moyo, P. *Concrete Repair, Rehabilitation and Retrofitting III: 3rd International Conference on Concrete Repair, Rehabilitation and Retrofitting, ICCRRR-3, Cape Town, South Africa, 3–5 September 2012*; CRC Press: London, UK, 2012.
4. Luković, M.; Šavija, B.; Dong, H.; Schlangen, E.; Ye, G. Micromechanical study of the interface properties in concrete repair systems. *J. Adv. Concr. Technol.* **2014**, *12*, 320–339. [CrossRef]
5. Fathy, A.; Zhu, H.; Kohail, M. Factors affecting the fresh-to-hardened concrete repair system. *Constr. Build. Mater.* **2022**, *320*, 126279. [CrossRef]
6. Qian, J.; You, C.; Wang, Q.; Wang, H.; Jia, X. A method for assessing bond performance of cement-based repair materials. *Constr. Build. Mater.* **2014**, *68*, 307–313. [CrossRef]
7. Zhou, J.; Ye, G.; Schlangen, E.; van Breugel, K. Modelling of stresses and strains in bonded concrete overlays subjected to differential volume changes. *Theor. Appl. Fract. Mech.* **2008**, *49*, 199–205. [CrossRef]
8. Hassan, K.; Brooks, J.; Al-Alawi, L. Compatibility of repair mortars with concrete in a hot-dry environment. *Cem. Concr. Compos.* **2001**, *23*, 93–101. [CrossRef]
9. Song, X.; Song, X.; Liu, H.; Huang, H.; Anvarovna, K.G.; Ugli, N.A.D.; Huang, Y.; Hu, J.; Wei, J.; Yu, Q. Cement-based repair materials and the interface with concrete substrates: Characterization, evaluation and improvement. *Polymers* **2022**, *14*, 1485. [CrossRef]
10. Shaw, M. *Guide to the Concrete Repair European Standards BS EN 1504 Series*; Sika Limited: Watchmead, Welwyn Garden City, Hertfordshire, UK, 2019.
11. El-Hawary, M.; Al-Khaiat, H.; Fereig, S. Performance of epoxy-repaired concrete in a marine environment. *Cem. Concr. Res.* **2000**, *30*, 259–266. [CrossRef]
12. Hunkeler, F. The resistivity of pore water solution—A decisive parameter of rebar corrosion and repair methods. *Constr. Build. Mater.* **1996**, *10*, 381–389. [CrossRef]
13. Basunbul, I.; Gubati, A.; Al-Sulaimani, G.; Baluch, M. Repaired reinforced concrete beams. *Mater. J.* **1990**, *87*, 348–354.
14. Saccani, A.; Magnaghi, V. Durability of epoxy resin-based materials for the repair of damaged cementitious composites. *Cem. Concr. Res.* **1999**, *29*, 95–98. [CrossRef]
15. Ariffin, N.F.; Hussin, M.W.; Sam, A.R.M.; Bhutta, M.A.R.; Khalid, N.H.A.; Mirza, J. Strength properties and molecular composition of epoxy-modified mortars. *Constr. Build. Mater.* **2015**, *94*, 315–322. [CrossRef]
16. Liu, Y.; Wang, F.; Liu, M.; Hu, S. A microstructural approach to adherence mechanism of cement and asphalt mortar (CA mortar) to repair materials. *Constr. Build. Mater.* **2014**, *66*, 125–131. [CrossRef]
17. Abu-Tair, A.; Rigden, S.; Burley, E. Testing the bond between repair materials and concrete substrate. *Mater. J.* **1996**, *93*, 553–558.
18. Lee, H.-S.; Park, J.-H.; Singh, J.K.; Ismail, M.A. Protection of reinforced concrete structures of waste water treatment reservoirs with stainless steel coating using arc thermal spraying technique in acidified water. *Materials* **2016**, *9*, 753. [CrossRef]
19. Lee, H.-S.; Park, J.-H.; Singh, J.K.; Ismail, M.A. Deposition of coating to protect waste water reservoir in acidic solution by arc thermal spray process. *Adv. Mater. Sci. Eng.* **2018**, *2018*, 4050175. [CrossRef]
20. Park, J.-H.; Singh, J.K.; Lee, H.-S. Ozone resistance, water permeability, and concrete adhesion of metallic films sprayed on a concrete structure for advanced water purification. *Coatings* **2017**, *7*, 41. [CrossRef]

21. Al-Negheimish, A.; Hussain, R.R.; Alhozaimy, A.; Singh, D. Corrosion performance of hot-dip galvanized zinc-aluminum coated steel rebars in comparison to the conventional pure zinc coated rebars in concrete environment. *Constr. Build. Mater.* **2021**, *274*, 121921. [CrossRef]
22. Lee, H.-S.; Singh, J.K.; Ismail, M.A.; Bhattacharya, C.; Seikh, A.H.; Alharthi, N.; Hussain, R.R. Corrosion mechanism and kinetics of Al–Zn coating deposited by arc thermal spraying process in saline solution at prolong exposure periods. *Sci. Rep.* **2019**, *9*, 3399. [CrossRef]
23. Lee, H.-S.; Kwon, S.-J.; Singh, J.K.; Ismail, M.A. Influence of Zn and Mg alloying on the corrosion resistance properties of Al coating applied by arc thermal spray process in simulated weather solution. *Acta Metall. Sin.* **2018**, *31*, 591–603. [CrossRef]
24. Lee, H.-S.; Park, J.-h.; Singh, J.K.; Choi, H.-J.; Mandal, S.; Jang, J.-M.; Yang, H.-M. Electromagnetic shielding performance of carbon black mixed concrete with Zn–Al metal thermal spray coating. *Materials* **2020**, *13*, 895. [CrossRef] [PubMed]
25. Choe, H.-B.; Lee, H.-S.; Shin, J.-H. Experimental study on the electrochemical anti-corrosion properties of steel structures applying the arc thermal metal spraying method. *Materials* **2014**, *7*, 7722–7736. [CrossRef] [PubMed]
26. Lee, H.-S.; Singh, J.K.; Park, J.H. Pore blocking characteristics of corrosion products formed on Aluminum coating produced by arc thermal metal spray process in 3.5 wt.% NaCl solution. *Constr. Build. Mater.* **2016**, *113*, 905–916. [CrossRef]
27. Steffens, H.-D.; Babiak, Z.; Wewel, M. Recent developments in arc spraying. *IEEE Trans. Plasma Sci.* **1990**, *18*, 974–979. [CrossRef]
28. Malek, M.H.A.; Saad, N.H.; Abas, S.K.; Shah, N.B.M. Critical process and performance parameters of thermal arc spray coating. *Int. J. Mater. Eng. Innov.* **2014**, *5*, 12–27. [CrossRef]
29. Davis, J.R. *Surface Engineering for Corrosion and Wear Resistance*; ASM International: Almere, The Netherlands, 2001.
30. *Korea Standard KS F4716*; Cement Filling Compound for Surface Preparation Korean Agency for Technology and Standards (KATS). Korean Agency for Technology and Standards: Eumseong County, Korea, 2001.
31. Lee, H.-S.; Singh, J.K. Deposition and corrosion studies of plasma arc thermal sprayed Zn and 85Zn–15Al films on steel surface. *J. Mater. Sci.* **2022**, *57*, 19650–19665. [CrossRef]
32. *Korea Standard KS F4930*; Penetrating Water Repellency of Liquid Type for Concrete Surface Application. Korea Standards Association: Seoul, Korea, 2002.
33. *Korea Standard KS F2584*; Standard Test Method for Accelerated Carbonation of Concrete. Korea Standards Association: Seoul, Korea, 2005.
34. Jang, J.-M.; Lee, H.-S.; Singh, J.K. Electromagnetic Shielding Performance of Different Metallic Coatings Deposited by Arc Thermal Spray Process. *Materials* **2020**, *13*, 5776. [CrossRef]
35. Sharifahmadian, O.; Salimijazi, H.; Fathi, M.; Mostaghimi, J.; Pershin, L. Study of the antibacterial behavior of wire arc sprayed copper coatings. *J. Therm. Spray Technol.* **2013**, *22*, 371–379. [CrossRef]
36. Deshpande, S.; Sampath, S.; Zhang, H. Mechanisms of oxidation and its role in microstructural evolution of metallic thermal spray coatings—Case study for Ni–Al. *Surf. Coat. Technol.* **2006**, *200*, 5395–5406. [CrossRef]
37. Cheng, X.; Roscoe, S.G. Corrosion behavior of titanium in the presence of calcium phosphate and serum proteins. *Biomaterials* **2005**, *26*, 7350–7356. [CrossRef]
38. Pouilleau, J.; Devilliers, D.; Garrido, F.; Durand-Vidal, S.; Mahé, E. Structure and composition of passive titanium oxide films. *Mater. Sci. Eng. B* **1997**, *47*, 235–243. [CrossRef]
39. Xie, M. Study of bond strength of composite and concrete interface in the rehabilitation of concrete structures using polymer composites. In Proceedings of the ICCM-X Vol. III: Process. Manufacturing; Woodhead Publishing: Vancouver, BC, Canada, 1995; pp. 613–620.
40. Karbhari, V.; Engineer, M. Investigation of bond between concrete and composites: Use of a peel test. *J. Reinf. Plast. Compos.* **1996**, *15*, 208–227. [CrossRef]
41. Shrestha, S.; Sturgeon, A. Use of advanced thermal spray processes for corrosion protection in marine environments. *Surf. Eng.* **2004**, *20*, 237–243. [CrossRef]
42. Zhu, Z.; Chu, H.; Guo, M.-Z.; Zhang, Y.; Song, Z.; Jiang, L. Anti-microbial corrosion performance of concrete treated by Cu_2O electrodeposition: Influence of different treatment parameters. *Cem. Concr. Compos.* **2021**, *123*, 104195. [CrossRef]
43. Ishikawa, T.; Matsumoto, K.; Yasukawa, A.; Kandori, K.; Nakayama, T.; Tsubota, T. Influence of metal ions on the formation of artificial zinc rusts. *Corros. Sci.* **2004**, *46*, 329–342. [CrossRef]
44. Amanian, S.; Naderi, R.; Mahdavian, M. The Role of an In-Situ Grown Zn-Al Layered Double Hydroxide Conversion Coating in the Protective Properties of Epoxy Coating on Galvanized Steel. *J. Electrochem. Soc.* **2022**, *169*, 031511. [CrossRef]